

On the Geochemistry and Mineralogy of the Anthropocene

Elhoucine Essefi^{1,2}

¹Higher Institute of Applied Sciences and Technology of Gabes, University of Gabes, Tunisia

²Unité de Recherche Electrochimie, Matériaux et Environnement UREME (UR17E545), Université de Gabès, Gabès, Tunisia

***Corresponding author:** Elhoucine Essefi, Higher Institute of Applied Sciences and Technology of Gabes, University of Gabes, Tunisia, E-mail: hocinsefi@yahoo.fr; hocinsefi@gmail.com

Received: 06 Apr, 2020 | **Accepted:** 27 May, 2020 | **Published:** 03 Jun, 2020

Citation: Essefi E (2020) On the Geochemistry and Mineralogy of the Anthropocene. *Int J Water Wastewater Treat* 6(2): dx.doi.org/10.16966/2381-5299.168

Copyright: © 2020 Essefi E. This is an open-access article distributed under the terms of the Creative Commons Attribution License, which permits unrestricted use, distribution, and reproduction in any medium, provided the original author and source are credited.

Abstract

Since geochemistry and mineralogy have been reciprocally controlled, this work is meant to review the setting of a geochemical and mineralogical signal related to the Anthropocene strata. From geochemical viewpoint, a worldwide geochemical enrichment of the atmosphere, hydrosphere and pedosphere may be used as stratigraphic markers of the Anthropocene. For instance, global biogeochemical cycles of major nutrient elements, trace elements, emerging pollutants, and organic pollutants were recently modified during the Anthropocene due to human activities. In addition, some isotopes may be used as an isotopic signature of widespread human impact on the global environment. Several methods were developed to evaluate the scale of anthropogenic effect including the computation of some geochemical parameters such as enrichment and contamination factors, geoaccumulation index and pollution load index. To make a distinction between natural and anthropogenic pollution, a geochemical background levels should be used. In addition, statistical methods such as Principal Component Analysis (PCA) and Clustering Technique (CT) argued relevant to study Anthropocene samples. As examples of Anthropocene record in Tunisian polluted sites, we presented three cases. (1) Record of the Anthropocene based on heavy metals and PCA along a core from the coast of Sfax. (2) Record of the Anthropocene based on infrared and CT along a core from Sebkha El Guetiate, Gabes. (3) Polychlorinated Biphenyls (PCBs) previously detected at the surface of Bizerte lagoon was reinterpreted as proxy to set the Anthropocene strata in Tunisian wetlands. Added to the direct effects of human pollution, secondary effects such as the acidification of aquatic environment increase mobility of several trace elements, leading hence to a new generation of mineral species. During a small period from 2017 to the beginning of the 2020, a boom of the number of mineral species may be noticed in the approved list of new minerals. In this review, we catalog only 30 mineral species resulting from combination of the new human induced elements pumped within environment.

Keywords: Anthropocene; Geochemistry; Mineralogy; Geochemical enrichment; Isotopic signature; Eleventh mineralogical stage; Human made mineral species

Introduction

The Anthropocene is an under discussion geologic epoch dating back to the setting of noticeable human direct and indirect impacts on terrestrial environments and subsequent geochemical and mineralogical repercussions [1,2]. Until now, the term Anthropocene is not approved as a formal subdivision of the geological scale [3]. In spite of the controversy on the Anthropocene starting date and its stratigraphic status, some common geochemical and mineralogical signals were recorded related to a polluted environment, changing climate and variable eustatism. Chemical contaminations are the most anthropogenic evident signals influencing the environment. Over decades, huge quantities of industrial and agricultural pollutants progressively enriched the atmosphere, hydrosphere, and pedosphere. In the vicinities of urban zones, anthropogenic contamination generally causes an elemental enrichment, compared with background levels, serving as chemostratigraphic markers of the Anthropocene. To set a new chronostratigraphic subdivision at the

beginning the Anthropocene, the signal should be persistent, sharp, global, and synchronous to indicate the required Global Stratotype Section and Point (GSSP).

Several proxies and methods were developed to evaluate the scale of anthropogenic effect including the computation of some geochemical parameters such as enrichment and contamination factors, geoaccumulation index and pollution load index. To make a distinction between natural and anthropogenic pollution, a geochemical background levels should be used. Combined with isotopic and geochemical signatures, anthropogenic contamination within dated cores may be used to set the Anthropocene-Holocene transition. Accordingly, certain elements may be used as geochemical proxy of increasing human activities. Added to the direct effects of human pollution, secondary effects such as the acidification of aquatic environment increase mobility of several trace elements. Over time, they have modified the natural cycles of chemical elements and caused direct and indirect repercussions on terrestrial systems.

Actually, the geochemistry and mineralogy could by no means be separately treated in the Anthropocene as well as in other chronostratigraphic subdivision. The geochemistry provides with all elemental ingredients to compile the chemical formula of any mineral. Furthermore, it controls chemical and physical parameters for enhancing the crystallization or the dissolution of minerals. In other words, the geochemistry not only it provides with necessary components of minerals but also it controls their domains of stability. Reciprocally, the dissolution of some minerals could enrich the environment by specific elements, creating hence a new geochemistry. For this reason, this work adopted a parallel investigation of Anthropocene geochemistry and mineralogy. One of the indirect repercussions of changing geochemistry during the Anthropocene is the appearance of a new mineralogy. This mineralogy is marked by the appearance of new mineral species as well as a change in the stability of already existing minerals. This change may lead to exceptional increasing amounts of some minerals and decreasing of others.

The aim of this work is twofold. On the one hand, it reviewed the geochemical signal of the Anthropocene worldwide recorded in the atmosphere as well as the hydrosphere and pedosphere. The best proxy and geochemical parameters used to record the Anthropocene were discussed. Several cases of geochemical record of the Anthropocene within Tunisian wetlands were presented. On the other hand, it reviewed the appearance of new mineralogy related to the combination of the newly introduced geochemical elements and the modified catalyzing environment. In addition, 30 additional mineral species recently approved by the International Mineralogical Association (IMA) (2018-2019-2020) updated the list of Anthropocene minerals.

Geochemistry of the Anthropocene

Encompassing different environmental systems (atmosphere, pedosphere, and biosphere) influenced on different scales (local, regional, global), human-environment interaction is complex and dynamic. Contrary to previous natural anomalies, Anthropocene anomalies recorded in recent sedimentary environments are due to pollution resulting from industrial sources. Although anthropogenic polluting elements travel through the atmosphere, hydrosphere, pedosphere and biosphere, they are finally best preserved in their natural outlet in archives of sedimentary environment [4]. Analytical chemistry coupled with geochemical methodology proves vital to distinguish between anthropogenic and natural origins [5,6]. Some of these methods and concepts used in geochemical exploration and environmental geochemistry may be used in the setting of the Anthropocene-Holocene transition based on geochemical anomalies [7] and reference therein. Nonetheless, geochemical anomalies should be first defined as abnormal values of elements concentrations compared with standard concentrations [8]. The evaluation of the geochemical background related to Anthropocene pollution was recently studied [9] and reference therein.

Elemental geochemistry

Due to a developing of analyses techniques leading to higher precision, elemental geochemistry is a good recorder for the setting of Anthropocene strata. The signal may be recorded on global as well as regional and local scales. According to the scale of the study and the used material and the analytical technique, scholars proposed different proxies to investigate the Anthropocene.

Biogeochemistry of nutrient elements: Global biogeochemical cycles of major nutrient elements on earth including C, N and P [10,11] (Figure 1) were recently modified during the Anthropocene

due to agricultural and industrial activities. Such anthropogenic pollution affecting the global carbon cycle has been widely discussed in the framework of climatic change and the increasing acidification of oceans [12]. Due an increasing anthropogenic CO₂, oceans acidification impacts the biogeochemistry of major nutrients on Earth. For instance, nitrogen fixation and denitrification increase in the nitrogen cycle [13], reducing hence the primary production [14]. These modifications would have repercussions on marine ecosystems fluctuations. The decrease in ocean pH causes under-saturation of CaCO₃, leading hence to coral reefs destruction [15,16]. Concentrations of soluble Fe in oceans increase due to the interaction between desert dust and anthropogenic acid aerosols. Since 1870, the increasing deposition of Fe-rich desert dust within regions of Fe deficiency enhanced nitrogen fixation oceans due to an intensified phytoplankton growth [17]. The global modification of the biogeochemical cycles basically started at the level of the atmosphere. Then, it propagates toward the other terrestrial systems. As the era of human modification, until now, the Anthropocene was not judged worthy a standalone subdivision within the geological scale. It seems that the human activity during the last decades is not considered until now at the rank to be compared with previous major events imposing a subdivision within the geological scale. Nonetheless, the exceptional environmental lesson of Corona virus showing a worldwide decrease of all pollutants in the atmosphere due to a diminution of industrial and agricultural activities during a small period argued that human effects on environment is not trivial. Accordingly, the epoch of anthropogenic effect is worthy to be individualized from the remaining Holocene part.

Trace elements: Scholars suggest marine rather continental environments to record trace elements enrichment [18,19]. Marine sediments are the best indicators of pollution. They are not influenced by pH, pE and other factors variations affecting trace elements mobility. It has been shown that trace elements concentrations in estuary sediments are strongly correlated with human activity related to traffic intensity and population density, serving hence as good stratigraphic markers of the Anthropocene.

Emerging pollutants: Not yet covered by existing regulations [20], this new trend of polluting substances may cause potential threats to ecosystems as well as human health. Some of them may be important indicators of the Anthropocene. The increasing use of these elements in medicinal and different high-technology industries caused their enrichment in the environment. In traditional wastewater treatment plants, their removal is difficult due to their persistence and weak biodegradability [20,21].

Isotope geochemistry

To investigate industrial pollution, stable isotopes of some elements were used [22]. Isotope signatures of S [23], Hg [24]; C [25], O [26] and N [27] may allow the record of polluting elements in environmental receptors as well as the location of emission sources. In addition, the specific isotope signature of a substance derived from a given source allows identification not only of its natural and/or anthropogenic origin but also it allows the tracing of the transport pathways [28]. Nonetheless, tracing the pathways and site of the anthropogenic pollution sources in complex ecosystems using stable isotopes is not straightforwardly feasible. For this reason, a multi-isotope approach [29-31] and combination with elemental signatures [32] may be useful. Global-scale enrichment of sediments in artificial radioisotopes such as ⁹⁰Sr [33], ¹³⁷Cs [34], ²³⁸Pu [35], ²³⁹Pu [36], ²⁴⁰Pu [37] and ²⁴¹Am [38] may help indicate indicating the starting date of the Anthropocene. The concentrations of the majority of these

radionuclides have increased since the starting of nuclear weapon testing [39,40]. From these studies, we can notice that, due to an increasing fuel consumption and fertiliser production, carbon and nitrogen isotope ratios increased during the 19th and 20th centuries. Lead and sulphur isotopes can be used to trace human pollution and acid rain, respectively. All these proxies may be used as an isotopic signature of widespread human impact on the global environment.

Organic geochemistry

With different structures (aliphatic, aromatic, polymers), organic pollutants are generally related to biogenic elements including in their structures C, H, and O. Following the pathways of biogeochemical cycles, they highly move across organic species integrated within the atmosphere, hydrosphere and pedosphere [41]. Due to their toxicity and residence time, Persistent Organic Pollutants (POP) have attracted researchers on marine [42] as well as continental [43] environments. Polycyclic Aromatic Hydrocarbons (PAHs) [44], Organochlorine Pesticides (OCs) [45], Polychlorinated Biphenyls (PCBs) [46], dioxins [47], polybrominated diphenyl ethers [48] and fluorinated compounds [49] may be used to set the Holocene-Anthropocene transition. Polychlorinated biphenyls not occurring in nature were worldwide produced and used from the onset the Anthropocene to cause radical change in sedimentary records. Actually, there is no record of known natural sources of the polychlorinated compounds [50]. They are globally transported, having hence a global dispersion in the remotest regions of the globe [51]; they show a very high persistence in the environment [52]. In addition, their affinity with sediments [53] provides a detectable signal over a long period.

Geochemical parameters

Several geochemical parameters were discussed for evaluation of human induced activities on environmental systems. Contamination indices were especially developed for concentrations of toxic trace metals (e.g. Zn, As, Cd, Cr, Hg, Cu) and persistent organic pollutants (e.g. polychlorinated biphenyls and polycyclic aromatic hydrocarbons). Related anthropogenic pollution, geochemical parameters are of relevant application to set the onset of Anthropocene. Pollution load index, index of geoaccumulation, Enrichment Factor (EF), and Contamination Factor (CF) are the possible candidate to record elemental enrichment during the Anthropocene.

Enrichment factor: As typical background enrichment index, it is one of the most commonly used geochemical parameters. It may be calculated as follow:

$$EF = (Ae \times Bc) / (Ac \times Be)$$

Ae is element concentration within the studied sample. Be is reference concentration of the element. Ac and Bc are the Clarke or average shale values of the studied element and the reference element respectively. The reference elements should be conservative having high resistance to weathering. The most often used as reference are the following elements: Al, Si, Fe, Sc, Li, Zr, Ti and Cs. Five categories may be found out based on EF values (Table 1) [54].

Contamination factor: First introduced by Hakanson L [55], Contamination Factor (CF) is the classification of the quality of sediments. Then, its use was extended to other applications including the valuation of soils and road dust. For calculation of the CF, we use the following formula:

$$CF = C_i / C_n$$

C_i is the mean concentration of the studied element within

samples from five different sampling sites. C_n is the background (pre-industrial or Clarke) concentration of the element. The evaluation of contamination is based on CFs values (Table 2).

In environmental studies, the use of more than one element is ensuring the evaluation of contamination. The degree of contamination CFs is calculated for more than one element. It is possible by summing CF values for eight pollutant species (Cd, As, Cr, Cu, Pb, Hg, Zn and polychlorinated biphenyls) to obtain a parameter known as the Degree of Contamination (Cdeg) [55,56] (Table 3).

Pollution load index: Pollution Load Index computing (PLI) [57] uses the concentration factors of different elements in the same sample (ConcF) with respect to its background value. It is an efficient tool to compare the pollution in different sites.

$$PLI = (\text{ConcF}_1 \times \text{ConcF}_2 \times \dots \times \text{ConcF}_n)^{1/n}$$

ConcF is a quotient of element concentration and its background concentration (Clarke or world average shale value). The PLI equal to 1 is the threshold between polluted and unpolluted samples. PLI values give information about pollution and the effectiveness of clean-up operations.

Index of geoaccumulation: Indeed, Geoaccumulation Index (Geo Index) is an efficient and simplest criterion to access heavy metal pollution. Muller G [58] determined the degree of sediments contamination with metal by comparing samples amounts with pre-industrial levels. It may be computed by the following equation. Geo Index = $\log_2(C_n / 1.5C_{bn})$. C_n is the metal (n) concentration in the

Table 1: Classification based Enrichment factor values.

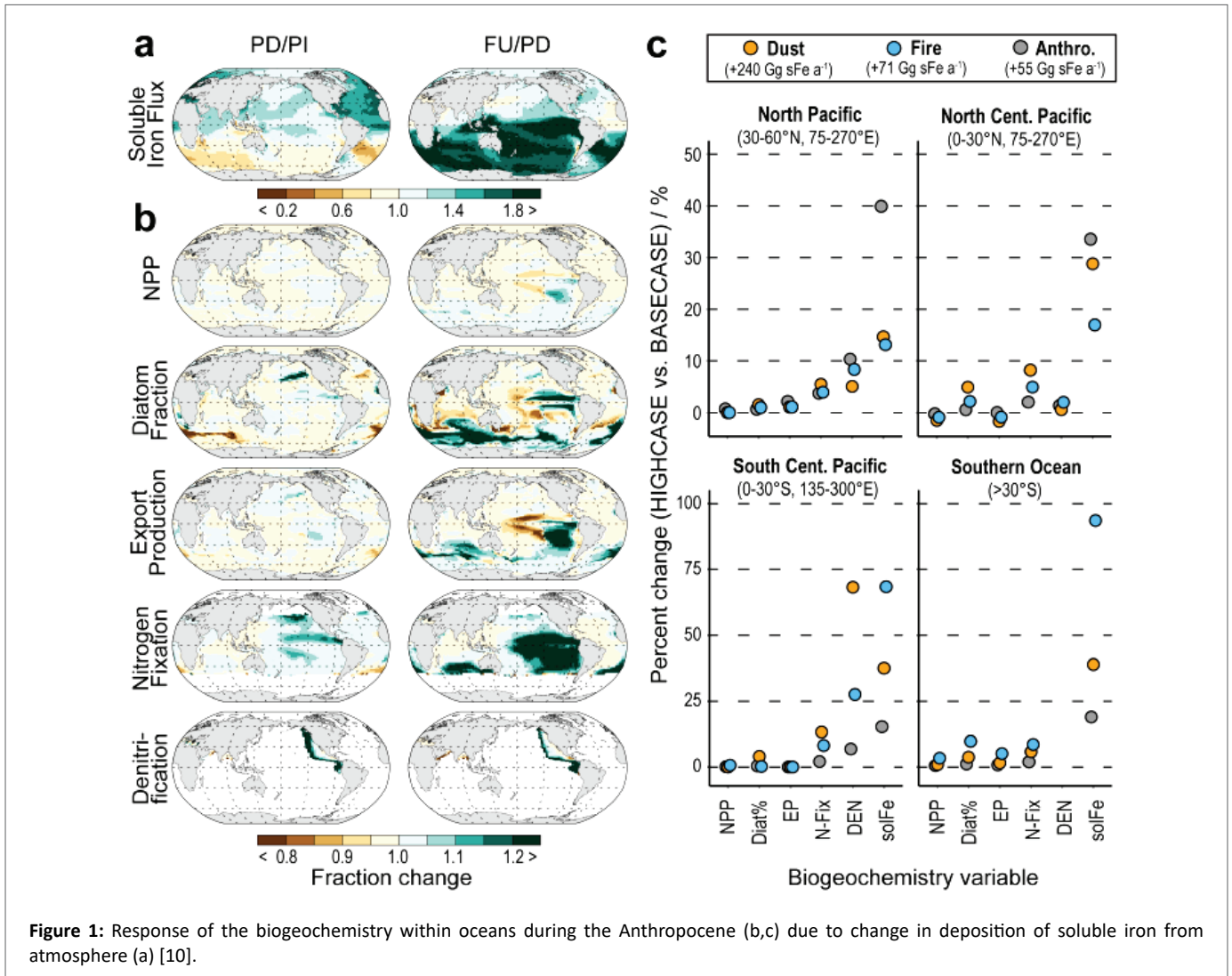
Enrichment factor values interval	Enrichment category
Less or equal to 2	Deficiency to minimal enrichment
[2,5]	Moderate enrichment
[5,20]	Significant enrichment
[20,40]	Very high enrichment
More than 40	Extremely high enrichment

Table 2: Types of contamination based on values of contamination factor.

Contamination factor values interval	Types of contamination
Less or equal to 1	Low contamination
[1,3]	Moderate contamination
[3,6]	Considerable contamination
More than 6	Very high contamination

Table 3: Degree of contamination.

Cdeg values interval	Degree of contamination
Less or equal to 8	Low contamination
[8,16]	Moderate contamination
[16,32]	Considerable contamination
More or equal to 6	Very high contamination



sediment and B_n is the background concentration of the metal (n), and 1.5 is the background matrix correction factor due to lithogenic effects. According to the Müller scale, the computed Geo Index related to the studied samples showed different classes of contamination (Table 4).

Statistical and computing techniques for Anthropocene signal detection

Detecting the Anthropocene does not deal only on analytical techniques. Instead, some statistical and computing methods may help in the individualization of anthropogenic samples as a standalone population. To name but a few, the Principal Component Analysis (PCA) and Clustering Techniques (CT). The mathematics of PCA and its use in environmental sciences has been widely discussed in the literature. This statistical technique has been proven relevant to find causal and genetic links between parameters monitoring pollution and their origins. Recent studies deals on the PCA to find the fingerprint of the Anthropocene strata [59]. On the other hand, coupled with PCA, clustering is a series of multivariate methods that is used to find 'true' groups of data, including samples or geochemical parameters. It is a widely used in many different disciplines such as biochemistry, biogeochemistry, biology and biometrics. Clustering Techniques

recently emerged as the most used to highlight pollution and follow its origins, allowing hence the identification of the Anthropocene strata [59].

Geochemical record of the Anthropocene within Tunisian sites

Heavy metal contamination in Tunisia wetlands: Wetlands are good recorder of the Anthropocene due to their fine grain size allowing heavy metals fixation and relative preservation of organic pollutants. In this work, we present a core from coast of Sfax (Southern Tunisia) showing an obvious setting of the Anthropocene strata. Based on Geoaccumulation Index (IGEO) values, anthropogenic activities have been shown to be responsible for significant contamination of sediments, particularly near coastal area. According to the results obtained, based on the geoaccumulation index of the metals measured, the values show a remarkable rise from the first ten centimeters of core (Figure 2). The geoaccumulation indexes of Pb and Cd are between 1 and 2, they are taken second class, and therefore the soil quality is moderately polluted. Cu and Ni have indexes that do not exceed value 1 and thereafter the soil quality is from unpolluted to moderately polluted. Generally, it can be seen that intensity of contamination is

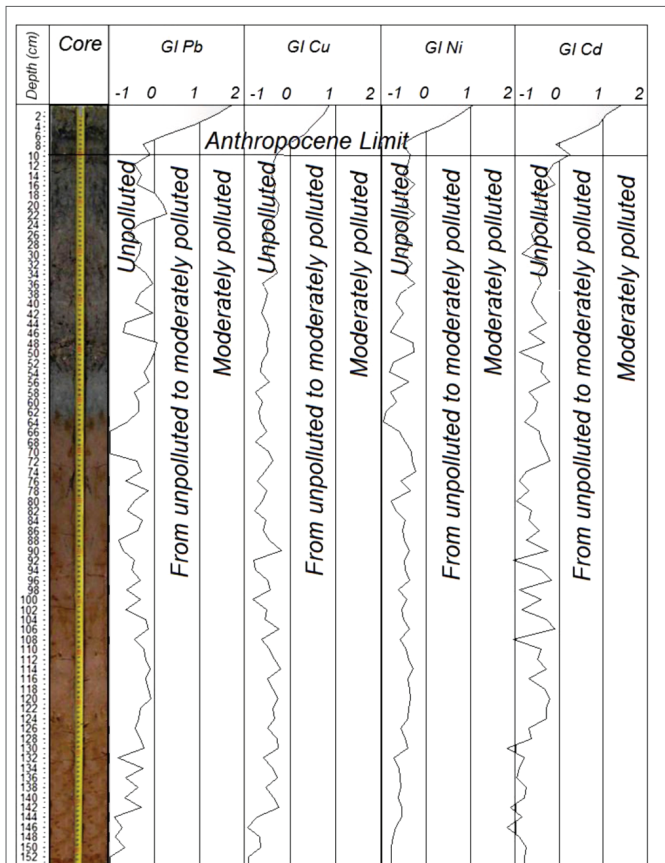


Figure 1: The setting of the Holocene-Anthropocene limit based on heavy metals along a core from the coast Sfax, southern Tunisia.

Table 4: Sediment classes according to Geo Index interval [58].

Geo Index interval	Class	Quality of sediment
Less or equal to 0	0	Unpolluted
[0,1]	1	From unpolluted to moderately polluted
[1,2]	2	Moderately polluted
[2,3]	3	From moderately to strongly polluted
[3,4]	4	Strongly polluted
[4,5]	5	From strongly to extremely polluted
More or equal to 5	6	Extremely polluted

moderately strong and the limit Anthropocene-Holocene is clearly remarkable in the upper part of core (from 10 cm).

The Principal Component Analysis PCA (Figure 3) of geochemical, sedimentary and geophysical parameters along the core from the coast of Sfax (Figure 2) shows the setting of two families. The first is basically natural induced and the second is related to human induced activities. The Pb related family is related to human activity. So, this family of parameters is a good indicator to set the Anthropocene strata.

Infrared and clustering technique to detect Anthropocene recorder in Tunisian wetlands: Infrared investigation of some cores from Tunisian wetlands shows the individualization of the tops of cores with obvious signature related to the setting of the Anthropocene.

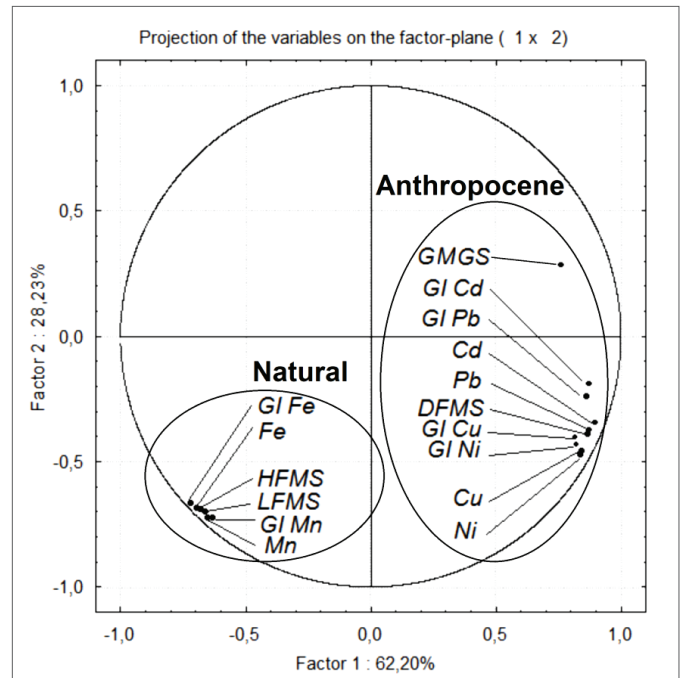


Figure 3: Principal Component Analysis PCA of some geochemical and geophysical parameters within a core from Tunisian coast.

The clustering of the infrared spectroscopy data (Figure 4) shows the individualization of the G5 (depth 2.5 cm) samples located at the upper part of the coastal sebkha of El Guetiate core (160 cm) (southern Tunisia). The setting of the Anthropocene at the top of this core is due to radical change of the sedimentary environment related climate change, pollution or variable eustatism. The investigation of infrared does not show obvious appearance of specific organic pollutants, probably due to their dilution within sediment or the weak limit of detection of this technique. Nonetheless, the CT individualizes the Anthropocene sample (G5) from the other remaining samples.

Polychlorinated Biphenyls as recorder of Anthropocene in Tunisian wetlands: Recently, some scholars [60] proposed Polychlorinated Biphenyls PCBs as a relevant stratigraphic marker of the Anthropocene strata. In Tunisia, PCBs was already recoded at the surface of the lagoon of Bizerte [61]. At Bizerte lagoon, 153, 138, and 180 PCBs are the predominant congeners (Figure 5). Taking into counts only teratogenel effects, the 209 PCB congeners are divided into (PCB Dioxine Like (PCB-DL) and PCB Non Nioxin Like (PCB-NDL). Comparable to dioxins, the PCBsDL have flat configuration. 12 of these congeners are considered the most toxic to health (4 ortho: 77, 81, 126 and 169; and 8 non-ortho: 105, 114, 118, 123, 156, 157, 167 and 189). However, they are the least abundant in mixtures industrial as in environmental matrices. In 1982, 7 indicator PCBs among the 209 congeners were selected by the Bureau European Commission Reference Community as compounds to be analyzed in priority within organic matrices in the pedosphere and biosphere due to their persistence, abundance as well as of their toxicological properties. Six PCBs-NDL (138, 153, 180, 28, 52 and 101) and one PCB-DL (118) considered as Indicator PCBs represent 80% of total PCBs. In Tunisia, the use of indicator PCBs represents promising perspectives for the setting of the Anthropocene strata.

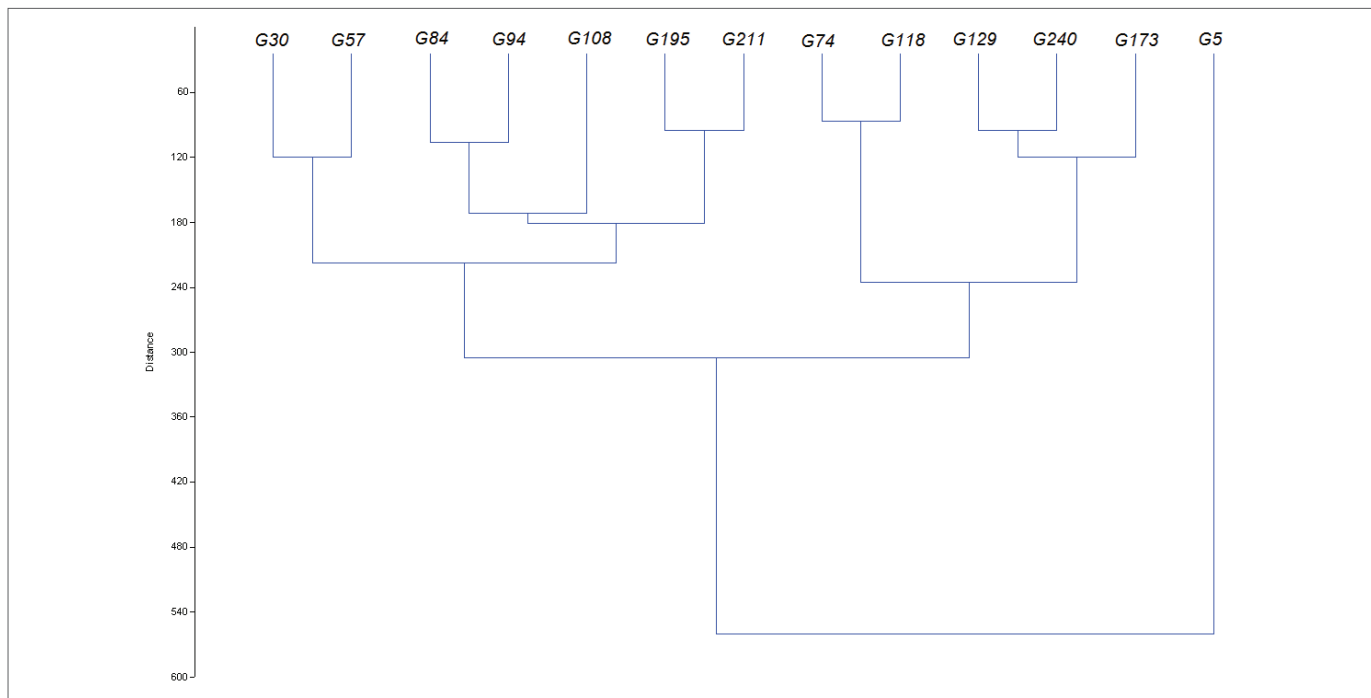
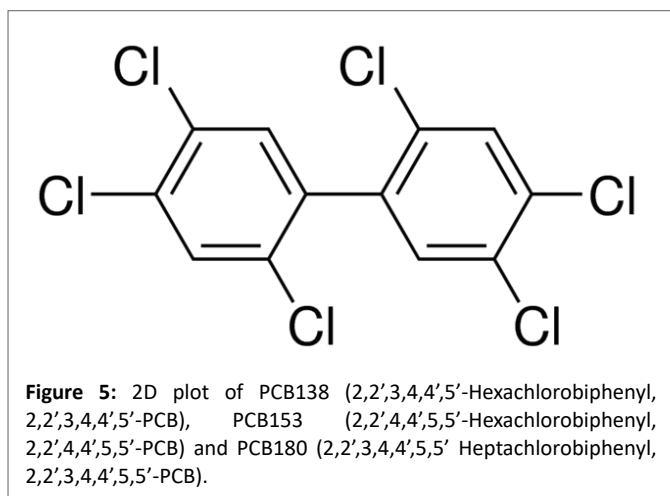


Figure 4: Clustering of the infrared spectroscopy data of a core from the seabed of El Guetiate, southern Tunisia: Anthropocene signal.



Emergence of New Mineral Species

Traditionally, minerals are natural compounds formed due to geological processes without any human intervention. Prior technological flourishing, 10 stages of mineral evolution were proposed [62]. Nonetheless, human-induced activities directly or indirectly resulted in the production of varied mineral-like compounds. In doing so, the Eleventh Stage is considered when the number of mineral species is experienced as a climax event related to the worldwide human effects during the Anthropocene (Figure 6) [62,63].

In fact, the persistence of a new Anthropocene geochemistry marked by enrichment with some chemical elements chronologically resulted in the setting of a new generation of Anthropocene minerals. The status of this Anthropocene mineralogy related to the *sensu stricto* definition of mineral has been controversially discussed due to serious

academic restrictions [63,64]. Nonetheless, attempts were carried out to enumerate the new mineral species related to the setting of the Anthropocene. Until 2017, 208 minerals related to the Anthropocene were cataloged [64]. During a small period from 2017 to the beginning of the 2020s, a boom in the number of mineral species may be noticed in the approved list of new minerals [65-72]. In this review, we catalog only 30 mineral species (Table 5 and Table 6), but other minerals may be included. This new mineralogy reflects the changing geochemistry by the appearance of trace elements, heavy metals, and phosphate groups in the formula of the combined minerals.

In this review, we present only eight mineral species (Figure 7 and Figure 8). Avdeevite ($\text{Na,Cs}(\text{Be}_2\text{Li})\text{Al}_2(\text{Si}_6\text{O}_{18})$) (Figure 7a) crystallizes in the hexagonal system. As for cell parameters, values are $a=9.2287$, $c=9.2610$ and the Ratio $a:c=1:1.003$. The unit cell volume is 683.08 \AA^3 . David brownite ($(\text{NH}_4)_5(\text{V}^{4+}\text{O})_2(\text{C}_2\text{O}_4)[\text{PO}_{2.75}(\text{OH})_{1.25}]_4 \cdot 3\text{H}_2\text{O}$) (Figure 7b) crystallizes in the monoclinic system. Cell parameters are $a=10.356$, $b=8.923$, $c=13.486$; $\beta=92.618^\circ$ Ratio: $a:b:c=1.161 : 1 : 1.511$; Unit Cell V: 1244.9 \AA^3 . In terms of physical properties, its color is light green-blue and the streak is white. On Mohs scale, the Hardness is 2. The measured density is 2.12 g/cm^3 . Kenngottite ($\text{Mn}^{2+}_3\text{Fe}^{3+}_4(\text{PO}_4)_4(\text{OH})_6(\text{H}_2\text{O})_2$) crystallizes in the monoclinic system (Figure 7c). Cell parameters are $a=13.909$, $b=5.186$, $c=12.159$; $\beta=98.88^\circ$, Ratio: $a:b:c=2.682 : 1 : 2.345$ Unit Cell V: 866.54 \AA^3 . Its hardness ranges between 4 and 5 on Mohs scale and the calculated density is equal to 3.40 g/cm^3 . Šlikite ($\text{Zn}_2\text{Mg}(\text{CO}_3)_2(\text{OH})_2 \cdot 4\text{H}_2\text{O}$) (Figure 7d) (Triclinic, Cell parameters: $a=6.335$, $b=6.340$, $c=13.923$; $\alpha=99.985^\circ$, $\beta=92.74^\circ$, $\gamma=114.93^\circ$ Ratio: $a:b:c=0.999:1 : 2.196$ Unit Cell V: 494.8 \AA^3). On Mohs scale, it has a hardness of 2.

The number of mineral species approved by the IAM commission is currently under revision. Nonetheless, the new mineralogy related to the Anthropocene is not only the appearance of new mineral species but also a modification of the abundance of already existing minerals. Also, the byproducts of several industrial, agricultural and nuclear

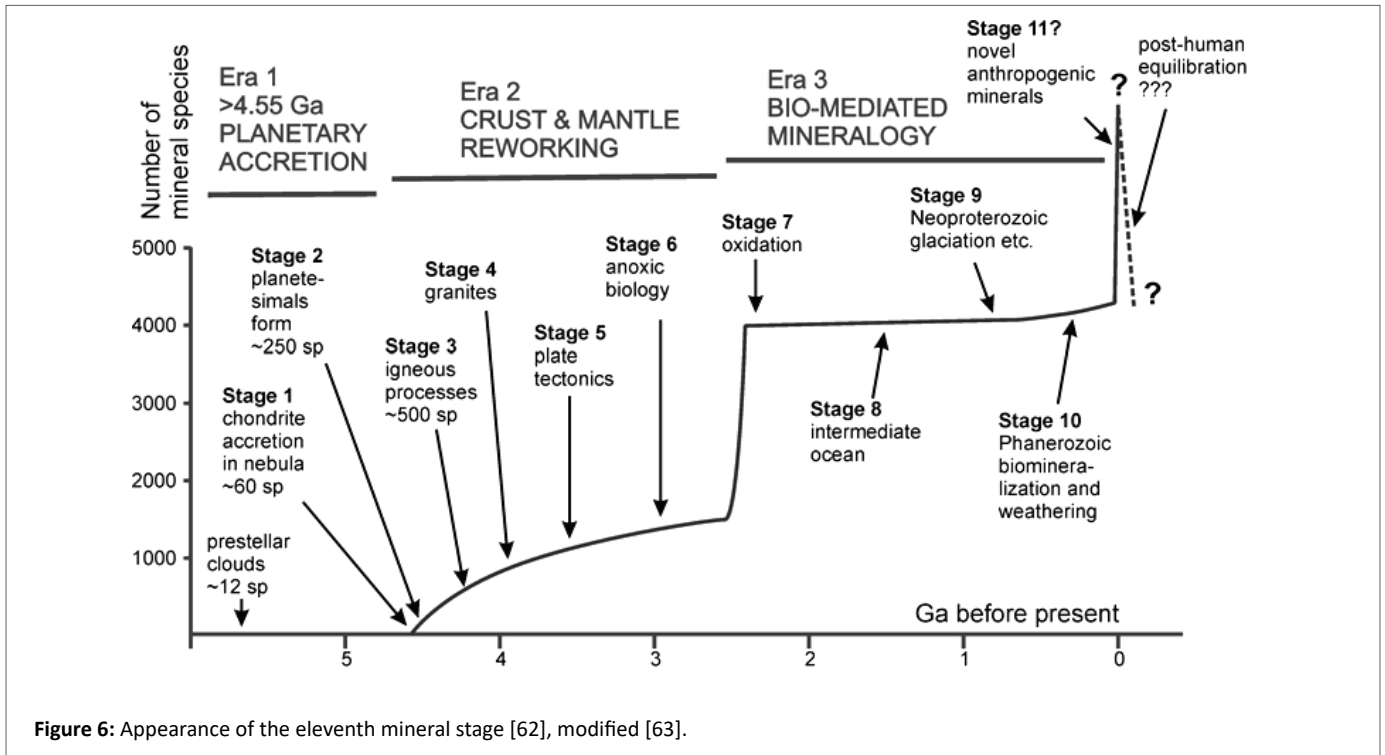


Figure 6: Appearance of the eleventh mineral stage [62], modified [63].

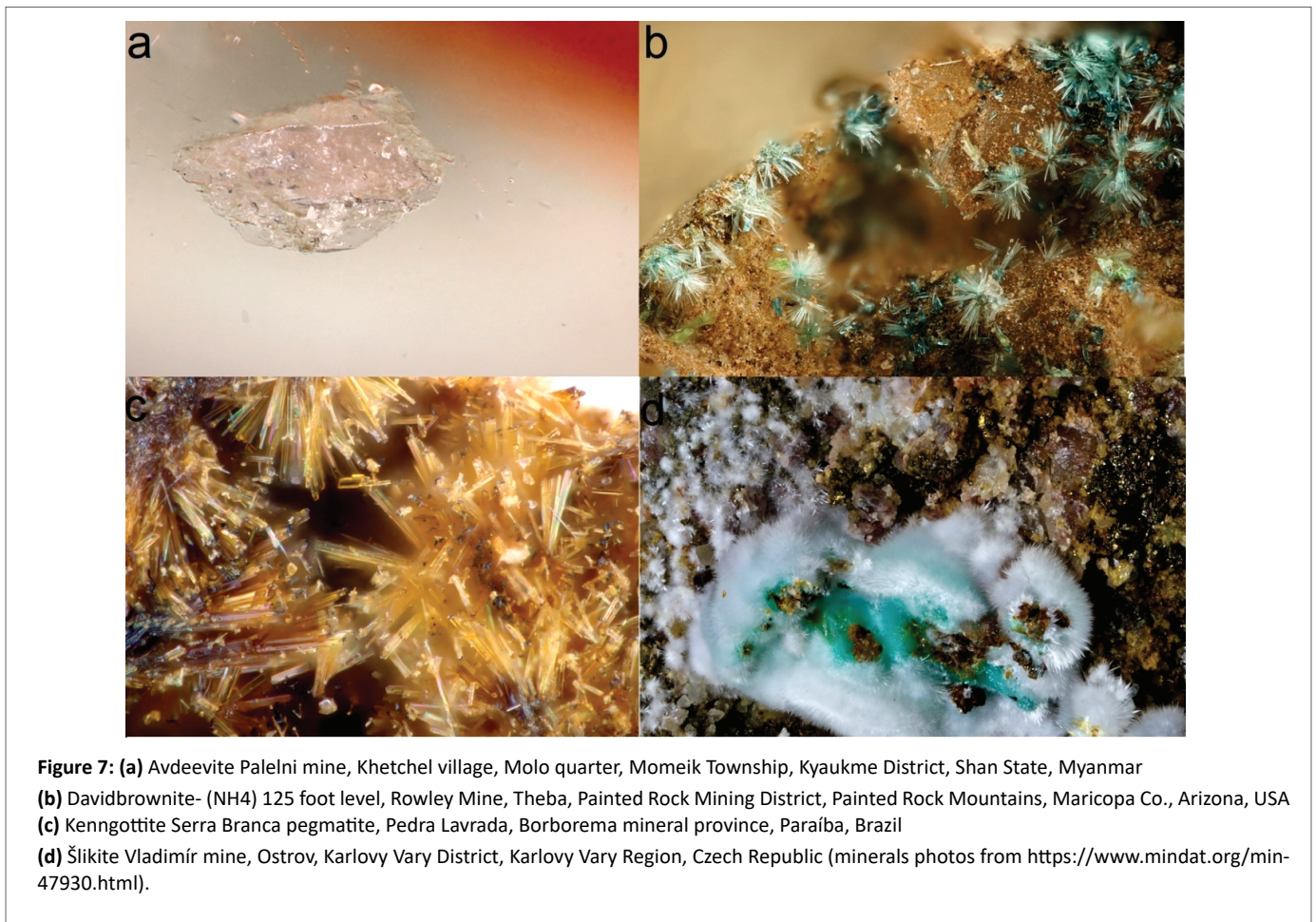


Figure 7: (a) Avdeevite Palelni mine, Khetchel village, Molo quarter, Momeik Township, Kyaukme District, Shan State, Myanmar
(b) Davidbrownite- (NH₄) 125 foot level, Rowley Mine, Theba, Painted Rock Mining District, Painted Rock Mountains, Maricopa Co., Arizona, USA
(c) Kenngottite Serra Branca pegmatite, Pedra Lavrada, Borborema mineral province, Paraíba, Brazil
(d) Šlikite Vladimír mine, Ostrov, Karlovy Vary District, Karlovy Vary Region, Czech Republic (minerals photos from <https://www.mindat.org/min-47930.html>).

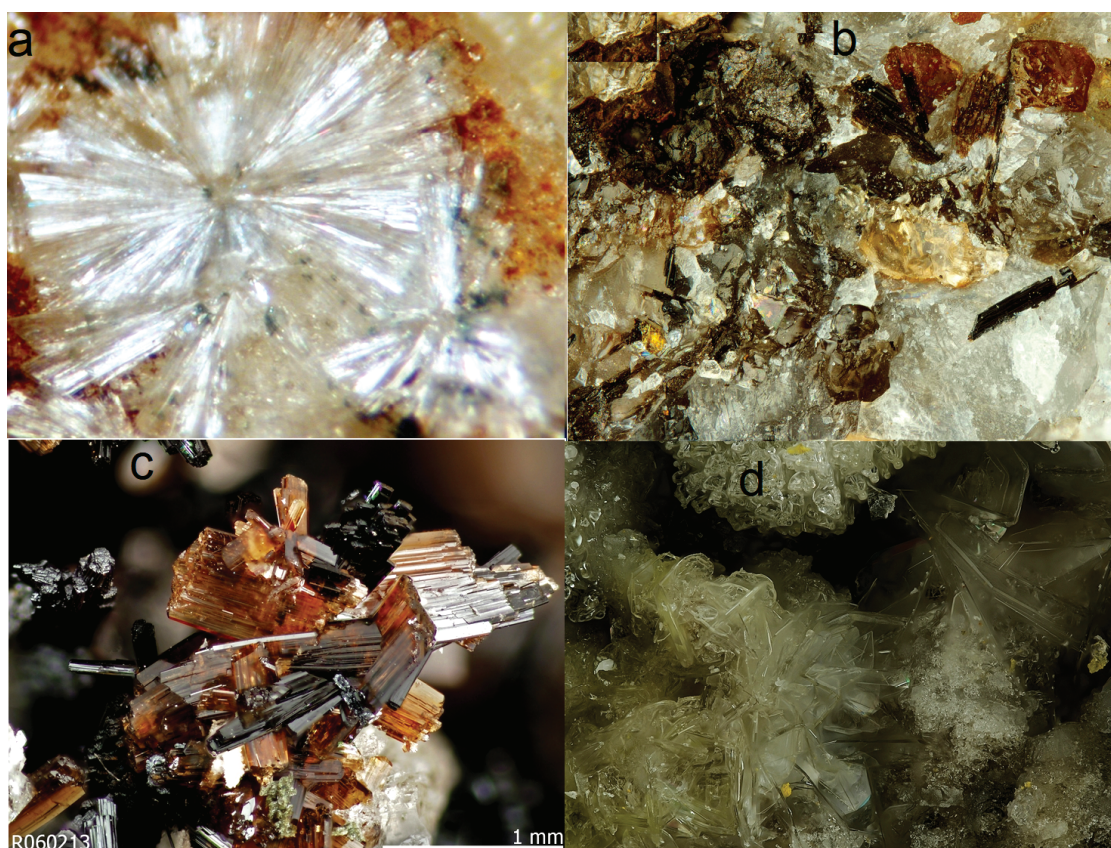


Figure 8: (a) Fanfaniite Foote Lithium Co. Mine, Kings Mountain Mining District, Cleveland Co., North Carolina, USA
(b) Folvikite, Kitteln Mine, Nordmark Odal Field, Filipstad, Värmland County, Sweden
(c) Jahnsite-(CaMnMg) Tip Top Mine, Fourmile, Custer Mining District, Custer Co., South Dakota, USA
(d) Russoite “Bocca Grande” fumarole, Solfatara di Pozzuoli, Pozzuoli, Naples, Campania, Italy (minerals photos from <https://www.mindat.org/min-47930.html>).

activities such as PO_4 , UO_2 , and BO_3 groups are integrated within the formula of majority of minerals in table 6. Some chemical elements classified as traces (e.g., Ti and Zr) or heavy metals (e.g., Fe and Mn) are imbedded within formula of these minerals. This enrichment of these new minerals with anthropogenic elements and functional groups advocates the strong link between Anthropocene geochemistry and mineralogy.

Fanfaniite, $(\text{Ca}_4\text{MnAl}_4(\text{PO}_4)_6(\text{OH})_4 \cdot 12\text{H}_2\text{O})$, is a phosphate mineral recorded at two localities: Foote spodumene mine, North Carolina, USA and the Hagendorf-Süd pegmatite, Bavaria, Germany. The presented example is from the USA (Figure 8a). With a radial form, the measured density is 2.58gcm^{-3} . Fanfaniite crystallizing in the monoclinic system, has a $C2/c$ space group, with $a=10.021 \text{ \AA}$, $b=24.137 \text{ \AA}$, $c=6.226 \text{ \AA}$, $\beta=91.54^\circ$ and $V=1505 \text{ \AA}^3$. Folvikite (Figure 8b) $(\text{Sb}^{5+}\text{Mn}^{3+}(\text{Mg},\text{Mn}^{2+})_{10}\text{O}_8(\text{BO}_3)_4)$ is Black to dark reddish-brown. The hardness on Mohs scale is 6. It crystallises in the monoclinic system. The calculated density is 4.14 g/cm^3 . Folvikite is an oxyborate mineral from the Kitteln mine, Värmland, Sweden. It occurs as a primary skarn mineral embedded in calcite. Jahnsite-(CaMnMg) (Figure 8c) $(\text{XM1M2}_2\text{M3}_2(\text{H}_2\text{O})_8(\text{OH})_2(\text{PO}_4)_4)$ is a funny nut brown and striated. These are distinct, nice crystals to 4 mm long, which is long for Jahnsite-(CaMnMg). The hardness is 4 and crystallizes in the monoclinic system. The measured density ranges between 2.706 and

2.718 g/cm^3 whereas the calculated is 2.715 g/cm^3 . Russoite (Figure 8d) $(\text{NH}_4)\text{ClAs}_2\text{O}_3(\text{H}_2\text{O})_{0.5}$ was found at the Solfatara di Pozzuoli, Pozzuoli, Napoli, Italy. It occurs as hexagonal plates up to $\sim 300 \mu\text{m}$ in diameter and $15 \mu\text{m}$ thick, in rosette-like intergrowths. The measured density is 2.89 g/cm^3 . On the other hand, the calculated density is 2.911 g/cm^3 . The mineral belongs to a small group of phylloarsenite minerals.

Conclusions

To standardize the Anthropocene as formal subdivision of the geological scale, geochemical and mineralogical markers of its starting date is required. Theoretically, all inorganic and organic pollutants can be used as indicators of anthropogenic activity. Nonetheless, they should satisfy certain criteria to provide with frank signals of the Anthropocene. With geographically extensive distribution extending on a global range, Anthropocene markers should record abrupt intensification related to Anthropocene setting with a permanent record. The chemical recording. Anthropocene strata are resulted from industrial and agricultural pollution as well as climatic and oceanographic changes. A major handicap of using these proxies lies in their deposition in the vicinity of industrial facilities. Another concern is related to their natural origin, representing hence a noise hiding the Anthropocene signal.

Table 5: Anthropocene minerals selected from the 2018-2019 list of new minerals approved by the IAM.

Name	Formula	Country	Approval year	Reference
Avdeevite	$(\text{Na,Cs})(\text{Be}_2\text{Li})\text{Al}_2(\text{Si}_6\text{O}_{18})$	Myanmar	2019	[73]
Bouškaite	$(\text{MoO}_2)_2\text{O}(\text{SO}_3\text{OH})_2(\text{H}_2\text{O})_4$	Czech Republic	2019	[74]
Davidbrowne-(NH4)	$(\text{NH}_4)_{1.5}(\text{V}^{4+}\text{O})_2(\text{C}_2\text{O}_4)_2[\text{PO}_{2.75}(\text{OH})_{1.25}]_4 \cdot 3\text{H}_2\text{O}$	USA	2019	[75]
Kenngottite	$\text{Mn}^{2+}_3\text{Fe}^{3+}_4(\text{PO}_4)_4(\text{OH})_6(\text{H}_2\text{O})_2$	Czech Republic	2019	[76]
Llantesite	$\text{Cu}_6\text{Al}[\text{SeO}_4]_2(\text{OH})_{12}\text{Cl} \cdot 3\text{H}_2\text{O}$	Argentina	2019	[77]
Magnesiobermanite	$\text{MgMn}^{3+}_2(\text{PO}_4)_2(\text{OH})_2 \cdot 4\text{H}_2\text{O}$	Australia	2018	[78]
Nickeltyrrellite	CuNi_2Se_4	Bolivia	2018	[79]
Nickolayite	FeMoP	Jordan	2019	[80]
Nikmelnikovite	$\text{Ca}_{12}\text{Fe}^{2+}\text{Fe}^{3+}_3\text{Al}_3(\text{SiO}_4)_6(\text{OH})_{20}$	Russia	2018	[81]
Ognitite	NiBiTe	Russia	2019	[82]
Orthocuproplatinum	Pt_3Cu	DR Congo	2019	[83]
Perbøeite-(La)	$\text{CaLa}_3(\text{AlAl}_2\text{Fe}^{2+})[\text{Si}_2\text{O}_7][\text{SiO}_4]_3\text{O}(\text{OH})_2$	Russia	2018	[84]
Pseudomarkeyite	$\text{Ca}_8(\text{UO}_2)_4(\text{CO}_3)_{12} \cdot 21\text{H}_2\text{O}$	USA	2018	[85]
Reaphookhillite	$\text{MgZn}_2(\text{PO}_4)_2 \cdot 4\text{H}_2\text{O}$	Australia	2019	[86]
Šlikite	$\text{Zn}_2\text{Mg}(\text{CO}_3)_2(\text{OH})_2 \cdot 4\text{H}_2\text{O}$	Czech Republic	2019	[87]
Stergiouite	$\text{CaZn}_2(\text{AsO}_4)_2 \cdot 4\text{H}_2\text{O}$	Greece	2019	[88]

Table 6: Anthropocene minerals recently published from 2019-2020 approved by the IAM.

Name	Formula	Country	Approval year	Reference
Chirvinskyite	$(\text{Na,Ca})_{13}(\text{Fe,Mn})_2(\text{Ti,Zr})_5(\text{Si}_2\text{O}_7)_4(\text{OH,O})_{12} \cdot 2\text{H}_2\text{O}$	Russia	2016	[89]
Fanfaniite	$\text{Ca}_4\text{MnAl}_4(\text{PO}_4)_6(\text{OH})_4 \cdot 12\text{H}_2\text{O}$	USA	2018	[90]
Folvikite	$\text{Sb}^{5+}\text{Mn}^{3+}(\text{Mg,Mn}^{2+})_{10}\text{O}_8(\text{BO}_3)_4$	Sweden	2016	[91]
Greenlizardite	$(\text{NH}_4)\text{Na}(\text{UO}_2)_2(\text{SO}_4)_2(\text{OH})_2 \cdot 4\text{H}_2\text{O}$	USA	2018	[92]
Horákite	$(\text{Bi}_7\text{O}_7\text{OH})[(\text{UO}_2)_4(\text{PO}_4)_2(\text{AsO}_4)_2(\text{OH})_2] \cdot 3.5\text{H}_2\text{O}$	Czech Republic	2017	[93]
Jahnsite Group	$\text{XM}_1\text{M}_2\text{M}_3(\text{H}_2\text{O})_8(\text{OH})_2(\text{PO}_4)_4$	Worldwide	2018	[94]
Kampelite	$\text{Ba}_6\text{Mg}_3\text{Sc}_6(\text{PO}_4)_{12}(\text{OH})_6 \cdot 7\text{H}_2\text{O}$	Russia	2016	[95]
Kuliginite	$\text{Fe}_3\text{Mg}(\text{OH})_6\text{Cl}_2$	Russia	2016	[96]
Mitrofanovite	Pt_3Te_4	Russia	2018	[97]
Plumbopharmacosiderite	$\text{Pb}_{0.5}\text{Fe}^{3+}_4(\text{AsO}_4)_4(\text{OH})_4 \cdot 5\text{H}_2\text{O}$	Italy	2016	[98]
Russoite	$(\text{NH}_4)\text{ClAs}_2\text{O}_3(\text{H}_2\text{O})_{0.5}$	Italy	2016	[99]
Siudaite	$\text{Na}_8(\text{Mn}^{2+}\text{Na})\text{Ca}_6(\text{Fe}^{3+}\text{Mn}^{2+})_3\text{Zr}_3\text{NbSi}_{24}(\text{Si,Ti})\text{O}_{74}(\text{OH})_2\text{Cl} \cdot 5\text{H}_2\text{O}$	Russia	2018	[100]
Smamite	$\text{Ca}_2\text{Sb}(\text{OH})_4[\text{H}(\text{AsO}_4)_2] \cdot 6\text{H}_2\text{O}$	France	2019	[101]
Bohuslavite	$\text{Fe}^{3+}_4(\text{PO}_4)_3(\text{SO}_4)(\text{OH}) \cdot n\text{H}_2\text{O}$ (15 ≤ n ≤ 24)	Italy	2019	[102]

Due to agricultural and industrial activities, global biogeochemical cycles of major nutrient elements on earth including C, N and P were recently modified during the Anthropocene. Due to their dispersion in the atmosphere far away from industrial sources, lead (Pb), mercury (Hg) and tin (Sn) are three metals whose biogeochemical cycles show the global-scale change caused by anthropogenic pollution.

As for the isotopic signature, due to an increasing fuel consumption and fertiliser production, carbon and nitrogen isotope ratios increased during the 19th and 20th centuries. Lead and sulphur isotopes can be used to trace human pollution and acid rain, respectively. All these proxies may be used as an isotopic signature of the Anthropocene strata.

In terms of organic geochemistry, Polycyclic Aromatic Hydrocarbons (PAHs), Organochlorine Pesticides (OCs), Polychlorinated Biphenyls (PCBs), dioxins, polybrominated diphenyl ethers and fluorinated compounds may be used to set the Holocene-Anthropocene transition.

Related anthropogenic pollution, geochemical parameters are of relevant application to set the onset of Anthropocene. Pollution load index, index of geoaccumulation, Enrichment Factor (EF), and Contamination Factor (CF) are the possible candidate to set background level and to record elemental enrichment during the Anthropocene.

Principal component analysis PCA and clustering techniques CT recently emerged as the most used to highlight pollution and follow its origins, allowing hence the identification of the Anthropocene strata.

As for the geochemical record of the Anthropocene within Tunisian sites, the Holocene-Anthropocene limit was set based on heavy metals along a core from the coast Sfax, southern Tunisia and the PCA of some geochemical and geophysical parameters. Clustering of the infrared spectroscopy data of a core from the sebkha of El Guetiate, southern Tunisia shows distinction of Anthropocene sample. PCBs (153, 138, and 180) already recorded at Bizerte lagoon are promising perspectives for the setting of the Anthropocene strata in Tunisian wetlands.

The Anthropocene is marked by unprecedented inorganic compounds emergency. In this review, we catalog only 30 mineral species approved by the International Mineralogical Association from 2017 to 2020. They are totally or partially occurring due to human activities. The setting of a new mineralogy is enhanced either *via* the setting of new geochemistry or *via* modification of global conditions controlling formation of new minerals and increasing the formation of the already existing minerals. The new geochemistry is richer with heavy metals and trace elements resulting hence in the precipitation of minerals containing in their formula these elements. On the other hand, the modification of global biogeochemical cycle enhanced the precipitation of some minerals and the dissolution of others.

References

- Zalasiewicz J, Waters CN, Williams M, Summerhayes CP (2019) The Anthropocene as a Geological Time Unit: A Guide to the Scientific Evidence and Current Debate. Cambridge University Press 156.
- Meszar M, Lappé K, Hornek K, Wagreich M (2019) Vienna's Anthropocene and anthropogenic geochemical signals. Geophysical Research Abstracts 21: EGU2019-10982.
- Castree N (2017) Unfree radicals: Geoscientists, the Anthropocene, and left politics. *Antipode* 49: 52-74.
- Foucher A, Evrard O, Cerdan O, Chabert C, Lecompte F, et al. (2020) A quick and low-cost technique to identify layers associated with heavy rainfall in sediment archives during the Anthropocene. *Sedimentology* 67: 486-501.
- Grygar TM, Popelka J (2016) Revisiting geochemical methods of distinguishing natural concentrations and pollution by risk elements in fluvial sediments. *J Geochem Explor* 170: 39-57.
- Gałuszka A, Migaszewski ZM, Namieśnik J (2017) The role of analytical chemistry in the study of the Anthropocene. *Trac-Trend Anal Chem* 97: 146-152.
- Seleznev AA, Yarmoshenko IV, Malinovsky GP (2020) Urban geochemical changes and pollution with potentially harmful elements in seven Russian cities. *Scientific Reports* 10: 1-16.
- Araújo PRM, Biondi CM, da Silva FBV, do Nascimento CWA, de Souza-Júnior VS (2018) Geochemical soil anomalies: Assessment of risk to human health and implications for environmental monitoring. *J Geochem Explor* 190: 325-335.
- García-Ordiales E, Flor-Blanco G, Roqueñí N, Covelli S, Cienfuegos P, et al. (2020) Anthropocene footprint in the Nalón estuarine sediments (northern Spain). *Mar Geol* 424: 106167.
- Hamilton DS, Moore JK, Arneth A, Bond TC, Carslaw KS, et al. (2020) Impact of Changes to the Atmospheric Soluble Iron Deposition Flux on Ocean Biogeochemical Cycles in the Anthropocene. *Global Biogeochem Cy* 34: e2019GB006448.
- Smith NJ, McDonald GW, Patterson MG (2020) Biogeochemical cycling in the anthropocene: Quantifying global environment-economy exchanges. *Ecol Model* 418: 108816.
- Hofmann M, Mathesius S, Krieglner E, van Vuuren DP, Schellnhuber HJ (2019) Strong time dependence of ocean acidification mitigation by atmospheric carbon dioxide removal. *Nature Communications* 10: 1-10.
- Wu D, Deng YF, Chen GH (2019) Developing a new thiosulfate-driven sulfur-cycle anammox process. 16th IWA world conference.
- Nizzoli D, Welsh DT, Viaroli P (2020) Denitrification and benthic metabolism in lowland pit lakes: The role of trophic conditions. *Sci Total Environ* 703: 134804.
- Morrison TH, Adger N, Barnett J, Brown K, Possingham H, et al. (2020) Advancing coral reef governance into the Anthropocene. *One Earth* 2: 64-74.
- Tebbett SB, Bellwood DR (2020) Sediments ratchet-down coral reef algal turf productivity. *Science of the Total Environment* 713: 136709.
- Bali K, Mishra AK, Singh S, Chandra S, Lehahn Y (2019) Impact of dust storm on phytoplankton bloom over the Arabian Sea: a case study during March 2012. *Environ Sci Pollut Res Int* 26: 11940-11950.
- Slaveykova VI (2019) Biogeochemical dynamics research in the Anthropocene. *Front Environ Sci* 7: 90.
- Kalisińska E (2019) Human Population Increase and Changes in Production and Usage of Trace Elements in the Twentieth Century and First Decades of the Twenty-First Century. *Mammals and Birds as Bioindicators of Trace Element Contaminations in Terrestrial Environments* 3-20.
- Delgado N, Capparelli A, Navarro A, Marino D (2019) Pharmaceutical emerging pollutants removal from water using powdered activated carbon: Study of kinetics and adsorption equilibrium. *J Environ Manag* 236: 301-308.
- Dharupaneedi SP, Nataraj SK, Nadagouda M, Reddy KR, Shukla SS, et al. (2019) Membrane-based separation of potential emerging pollutants. *Sep Purif Technol* 210: 850-866.
- Novak M, Holmden C, Farkaš J, Kram P, Hruska J, et al. (2020) Calcium and strontium isotope dynamics in three polluted forest ecosystems of the Czech Republic, Central Europe. *Chem Geol* 536: 119472.
- Olson EJ, Michalski G, Welp LR, Larrea Valdivia A, Reyes J, et al. (2019) Sulfur Isotope Constraints on PM 2.5 Sulfate Aerosol Sources in Arequipa, Peru. *American Geophysical Union A23K-2926*.
- Broczka FM, Biester H, Richard JH, Kraemer SM, Wiederhold JG (2019) Mercury Isotope Fractionation in the Subsurface of a Hg (II) Chloride-Contaminated Industrial Legacy Site. *Environ Sci Technol* 53: 7296-7305.
- Hong S, Lee Y, Yoon SJ, Lee J, Kang S, et al. (2019) Carbon and nitrogen stable isotope signatures linked to anthropogenic toxic substances pollution in a highly industrialized area of South Korea. *Marine pollution bulletin* 144: 152-159.
- Gruber R, Chan N, Heiling M, Adu-Gyamfi J, Heng L, et al. (2019) Oxygen isotopes in phosphate to study soil P fractions and to trace sources of pollutants in agricultural catchment. 21st EGU General Assembly.
- de Carvalho DR, Alves CBM, Flecker AS, Sparks JP, Moreira MZ, et al. (2020) Using $\delta^{15}N$ of periphyton and fish to evaluate spatial and seasonal variation of anthropogenic nitrogen inputs in a polluted Brazilian river basin. *Ecological Indicators* 115: 106372.

28. Preziosi E, Frollini E, Zoppini A, Ghergo S, Melita M, et al. (2019) Disentangling natural and anthropogenic impacts on groundwater by hydrogeochemical, isotopic and microbiological data: Hints from a municipal solid waste landfill. *Waste management* 84: 245-255.
29. Souto-Oliveira CE, Babinski M, Araújo DF, Weiss DJ, Ruiz IR (2019) Multi-isotope approach of Pb, Cu and Zn in urban aerosols and anthropogenic sources improves tracing of the atmospheric pollutant sources in megacities. *Atmos Environ* 198: 427-437.
30. Zhang Q, Wang H (2020) Assessment of sources and transformation of nitrate in the alluvial-pluvial fan region of north China using a multi-isotope approach. *J Environ Sci* 89: 9-22.
31. Halder J, Akpataku KV, Bawa LM, Djaneye-Boundjou G, Faye S (2019) Multi-isotope approach to identify sources and fate of nitrate in the Plateaux Region of Togo. *Geophysical Research Abstracts* 21: EGU2019-18788.
32. Romo-Morales D, Moreno-Rodríguez V, Molina-Freaner F, Valencia-Moreno M, Ruiz J, et al. (2020) Assessment of Geogenic and Anthropogenic Pollution Sources Using an Aquatic Plant Along the Sonora River Basin: Insights from Elemental Concentrations and Pb Isotope Signatures. *Natural Resources Research* 1-14.
33. Kalinichenko SA, Nikitin AN, Cheslyk IA, Shurankova OA (2020) Spatial Distribution of ^{90}Sr in the Ecosystems of Polesye State Radiation-Ecological Reserve. *Strontium Contamination in the Environment* 121-140.
34. Maruo YY (2019) Air pollution monitoring network of $\text{PM}_{2.5}$, NO_2 and radiation of ^{137}Cs . *Chemical, Gas, and Biosensors for Internet of Things and Related Applications* 323-338.
35. Kierepko R, Sahoo SK, Hosoda M, Tokonami S, Sorimachi A, et al. (2019) $^{238}\text{Pu}/(^{239+240}\text{Pu})$ activity ratio as an indicator of Pu originating from the FDNPP accident in the terrestrial environment of Fukushima Prefecture. *J Environ Radioact* 196: 133-140.
36. Jacobson MZ (2019) Evaluation of Nuclear Power as a Proposed Solution to Global Warming, Air Pollution, and Energy Security. Cambridge University Press.
37. Huang Y, Tims SG, Froehlich MB, Pan S, Fifield LK, et al. (2019) The $^{240}\text{Pu}/^{239}\text{Pu}$ Atom Ratio in Chinese Soils. *Sci Total Environ* 678: 603-610.
38. Kashirsky V, Shatrov A, Zvereva I, Lukashenko S (2020) Development of a Method for Studying $^{241}\text{Pu}/^{241}\text{Am}$ Activity Ratio in the Soil of the Main Semipalatinsk Test Site Areas. *J Environ Radioact* 216: 106181.
39. Johansen MP, Child DP, Cresswell T, Harrison JJ, Hotchkis MAC, et al. (2019) Plutonium and Other Radionuclides Persist Across Marine-To-Terrestrial Ecotopes in the Montebello Islands Sixty Years after Nuclear Tests. *Sci Total Environ* 691: 572-583.
40. Drozdovitch V, de Vathaire F, Bouville A (2020) Ground Deposition of Radionuclides in French Polynesia Resulting From Atmospheric Nuclear Weapons Tests at Mururoa and Fangataufa Atolls. *J Environ Radioact* 214-215: 106176.
41. Tian BB, Zhou JH, Xie F, Guo QN, Zhang AP, et al. (2019) Impact of surfactant and dissolved organic matter on uptake of atrazine in maize and its mobility in soil. *J soils sediments* 19: 599-608.
42. Balmer B, Ylitalo G, Watwood S, Quigley B, Bolton J, et al. (2019) Comparison of Persistent Organic Pollutants (POPs) Between Small Cetaceans in Coastal and Estuarine Waters of the Northern Gulf of Mexico. *Mar Pollut Bull* 145: 239-247.
43. Ontiveros-Cuadras JF, Ruiz-Fernández AC, Sanchez-Cabeza JA, Sericano J, Pérez-Bernal LH, et al. (2019) Recent History of Persistent Organic Pollutants (PAHs, PCBs, PBDEs) in Sediments from a Large Tropical Lake. *J Hazard Mater* 368: 264-273.
44. Lubecki L, Oen AMP, Breedveld GD, Zamojska A (2019) Vertical profiles of sedimentary polycyclic aromatic hydrocarbons and black carbon in the Gulf of Gdańsk (Poland) and Oslofjord/Drammensfjord (Norway), and their relation to regional energy transitions. *Science Total Environ* 646: 336-346.
45. Wang C, Hao Z, Feng Z, Zhang C, Gao J, et al. (2020) Rapid changes in organochlorine pesticides in sediments from the East China sea and response to human-induced catchment changes. *Water Res* 169: 115225.
46. Quadra GR, Teixeira JRPVA, Barros N, Roland F, Amado AM (2019) Water pollution: one of the main Limnology challenges in the Anthropocene. *Acta Limnol Bras* 31.
47. Marinaro J, Tanrikut C (2019) Environmental Toxins and Men's Health. In *Effects of Lifestyle on Men's Health*. Academic Press 363-401.
48. Cetin B, Yurdakul S, Odabasi M (2019) Polybrominated diphenyl ethers (PBDEs) pollution in soil of a highly industrialized region (Dilovasi) in Turkey: concentrations, spatial and temporal variations and possible sources. *Environ Monit Assess* 191: 474.
49. Lim XZ (2019) Tainted Water: The Scientists Tracing Thousands of Fluorinated Chemicals in Our Environment. *Nature* 566: 26-29.
50. Nair S, Abraham J (2019) Biodegradation of Polychlorinated Biphenyls. In: Arora PK (eds) *Microbial Metabolism of Xenobiotic Compounds*. Springer, Singapore 263-284.
51. Liu C, Wei BK, Bao JS, Wang Y, Hu JC, et al. (2020) Polychlorinated biphenyls in the soil-crop-atmosphere system in E-waste dismantling areas in Taizhou: Concentrations, congener profiles, uptake, and translocation. *Environ Pollut* 257: 113622.
52. Li X, Dong S, Wang P, Su X, Fu J (2019) Polychlorinated biphenyls are still alarming persistent organic pollutants in marine-origin animal feed (fishmeal). *Chemosphere* 233: 355-362.
53. Fraser MA, Chen L, Ashar M, Huang W, Zeng J, et al. (2020) Occurrence and distribution of microplastics and polychlorinated biphenyls in sediments from the Qiantang River and Hangzhou Bay, China. *Ecotoxicol Environ Saf* 196: 110536.
54. Halstead MJR, Cunnigham RG, Hunter KA (2000) Wet deposition of trace metals to a remote site in Fjordland, New Zealand. *Atmos Environ* 34: 665-676.
55. Hakanson L (1980) An ecological risk index for aquatic pollution control: a sedimentological approach. *Water Res* 14: 975-1001.
56. Diatta JB, Chudzinska E, Wirth S (2008) Assessment of heavy metal contamination of soils impacted by a zinc smelter activity. *J Elementol* 13: 5-16.
57. Tomlinson DL, Wilson JG, Harris CR, Jeffrey DW (1980) Problems in the assessment of heavy-metal levels in estuaries and the formation of a pollution index. *Helgol Mar Res* 33: 566-575.
58. Müller G, Putz G (1969) Index of geoaccumulation in sediments of the Rhine River. *J Geol* 2: 108-118.
59. Gałuszka A, Migaszewski ZM, Rose NL (2020) A consideration of polychlorinated biphenyls as a chemostratigraphic marker of the Anthropocene. *Anthropocene Rev* 2053019620916488.

60. Aliff MN, Reavie ED, Post SP, Zanko LM (2020) Anthropocene geochemistry of metals in sediment cores from the Laurentian Great Lakes. *Peer J* 8: e9034.
61. Barhoumi B, LeMenach K, Dévier MH, El megdiche Y, Hammami B, et al. (2014) Distribution and ecological risk of polychlorinated biphenyls (PCBs) and organochlorine pesticides (OCPs) in surface sediments from the Bizerte lagoon, Tunisia. *Environ Sci Pollut Res* 21: 6290-6302.
62. Hazen RM, Papineau D, Bleeker W, Downs RT, Ferry J, et al. (2008) Mineral evolution. *Am Mineral* 93: 1693-1720.
63. Zalasiewicz J, Kryza R, Williams M (2013) The mineral signature of the Anthropocene in its deep-time context. *Geological Society, London, Special Publications* 395: 109-117.
64. Hazen RM, Grew ES, Origlieri MJ, Downs RT (2017) On the mineralogy of the "Anthropocene Epoch". *Am Mineral* 102: 595-611.
65. Miyawaki R, Hatert F, Pasero M, Mills SJ (2019) IMA Commission on New Minerals, Nomenclature and Classification (CNMNC) NEWSLETTER 50: New minerals and nomenclature modifications approved in 2019. *Eur J Mineral* 31: 847-853.
66. Miyawaki R, Hatert F, Pasero M, Mills SJ (2019) IMA Commission on New Minerals, Nomenclature and Classification (CNMNC) NEWSLETTER 48: New minerals and nomenclature modifications approved in 2019. *Eur J Mineral* 31: 399-402.
67. Miyawaki R, Hatert F, Pasero M, Mills MJ (2019) IMA Commission on New Minerals, Nomenclature and Classification (CNMNC) NEWSLETTER 51: New minerals and nomenclature modifications approved in 2019. *Eur J Mineral* 31: 1099-1104.
68. Miyawaki R, Halenius U, Hatert F, Pasero M, Mills SJ (2019) IMA Commission on New Minerals, Nomenclature and Classification (CNMNC) NEWSLETTER 47: New minerals and nomenclature modifications approved in 2018 and 2019. *Eur J Mineral* 31: 197-202.
69. Miyawaki R, Hatert F, Pasero M, Mills SJ (2020) IMA Commission on New Minerals, Nomenclature and Classification (CNMNC)-Newsletter 54. *Eur J Mineral* 32: 275-283.
70. Miyawaki R, Hatert F, Pasero M, Mills SJ (2020) IMA Commission on New Minerals, Nomenclature and Classification (CNMNC)-Newsletter 53. *Eur J Mineral* 32: 209-213.
71. Miyawaki R, Hatert F, Pasero M, Mills SJ (2020) IMA Commission on New Minerals, Nomenclature and Classification (CNMNC)-Newsletter 52. *Eur J Mineral* 32: 1-11.
72. Miyawaki R, Halenius U, Hatert F, Pasero M, Mills SJ (2019) New minerals and nomenclature modifications approved in 2018 and 2019. *Mineral Mag* 83: 143-147.
73. Agakhanov AA, Stepanenko DA, Zubkova NV, Pekov IV, Pautov LA, et al. (2019) Avdeevite, IMA 2018-109. *CNMNC Newsletter No. 47. Eur J Mineral* 31: 199-204.
74. Sejkora J, Grey IE, Kampf AR, Plášil J, Škácha P (2019) Bouškaite, a new molybdenyl-hydrogensulfate mineral, $(\text{MoO}_2)_2\text{O}(\text{SO}_3\text{OH})_2(\text{H}_2\text{O})_2 \cdot 2\text{H}_2\text{O}$, from the Lill mine, Příbram ore area, Czech Republic. *J Geol* 64: 197-205.
75. Kampf AR, Cooper MA, Rossman GR, Nash BP, Hawthorne FC, et al. (2019) Davidbrownite- (NH_4) , $(\text{NH}_4, \text{K})_5(\text{V}^{4+}\text{O})_2(\text{C}_2\text{O}_4)[\text{PO}_{2.75}(\text{OH})_{1.25}]\cdot 3\text{H}_2\text{O}$, a new phosphate-oxalate mineral from the Rowley mine, Arizona, USA. *Mineral Mag* 83: 869-877.
76. Sejkora J, Grey IE, Kampf AR (2019) Kenngottite, $\text{Mn}^{2+}_3\text{Fe}^{3+}_4(\text{PO}_4)_4(\text{OH})_6(\text{H}_2\text{O})_2$, a new phosphate mineral from Krásno near Horní Slavkov, Czech Republic. *Eur J Mineral* 31: 629-636.
77. Lengauer CL, Ende M, Topa D, Lira R, Paar WH (2019) Llantenesite, IMA 2018-111. *CNMNC Newsletter No. 47. Eur J Mineral* 31: 199-204.
78. Elliott P (2019) Magnesiobermanite, IMA 2018-115. *CNMNC Newsletter No. 47. Eur J Mineral* 31: 199-204.
79. Förster HJ, Ma C, Grundmann G, Bindi L, Stanley CJ (2019) Nickeltyrrellite, CuNi_2Se_4 , a New Member of the Spinel Supergroup from El Dragón, Bolivia. *Can Mineral* 57: 637-646.
80. Murashko MN, Vapnik Y, Polekhovskiy YP, Shilovskikh VV, Zaitsev AM, et al. (2019) Nickolayite, IMA 2018-126. *CNMNC Newsletter No. 47. Eur J Mineral* 31: 199-204.
81. Krivovichev SV, Yakovenchuk VN, Panikorovskii TL, Savchenko EE, Pakhomovsky YA, et al. (2019) Nikmelnikovite, IMA 2018-043. *CNMNC Newsletter No. 47. Eur J Mineral* 31: 199-204.
82. Barkov AY, Bindi L, Tamura N, Shvedov GI, Winkler B, et al. (2019) Ognitite, NiBiTe, a new mineral species, and Co-rich maucherite from the Ognit ultramafic complex, Eastern Sayans, Russia. *Mineral Mag* 83: 695-703.
83. Cabral AR, Skála R, Vymazalová A, Maixner J, Stanley CJ, et al. (2019) Orthocuproplatinum, Pt_3Cu , a new mineral from the Lubero region, North Kivu, Democratic Republic of the Congo. *Mineral Petrol* 113: 527-532.
84. Kasatkin AV, Pekov IV, Zubkova NV, Chukanov NV, Škoda R, et al. (2019) Perbøeite-(La), IMA 2018-116. *CNMNC Newsletter No. 47. Eur J Mineral* 31: 199-204.
85. Kampf AR, Olds TA, Plášil J, Burns PC, Marty J (2019) Pseudomarkeyite, IMA 2018-114. *CNMNC Newsletter No. 47. Eur J Mineral* 31: 199-204.
86. Elliott P (2019) Reaphookhillite, IMA 2018-128. *CNMNC Newsletter No. 47. Eur J Mineral* 31: 199-204.
87. Sejkora J, Grey IE, Kampf AR, Mumme WG, Bureš B, et al. (2019) Šlikite, $\text{Zn}_2\text{Mg}(\text{CO}_3)_2(\text{OH})_2 \cdot 4\text{H}_2\text{O}$, a new Zn-Mg carbonate from Plavno, Jáchymov ore district, Czech Republic. *Eur J Mineral* 31: 1047-1054.
88. Rieck B, Giester G, Lengauer LC, Chanmuang C, Topa D (2020) Stergiouite, $\text{CaZn}_2(\text{AsO}_4)_2 \cdot 4\text{H}_2\text{O}$ - a new mineral from the Lavrion Mining District, Greece. *Mineral Petrol* 214783764.
89. Yakovenchuk VN, Pakhomovsky YA, Panikorovskii TL, Zolotarev AA, Mikhailova JA, et al. (2019) Chirvinskyite, $(\text{Na,Ca})_{13}(\text{Fe,Mn})_2(\text{Ti,Nb})_2(\text{Zr,Ti})_3(\text{Si}_2\text{O}_7)_4(\text{OH,O,F})_{12}$, a New Mineral with a Modular Wallpaper Structure, from the Khibiny Alkaline Massif (Kola Peninsula, Russia). *Minerals* 9: 219.
90. Roattino T, Meisser N, Iob S, Berbain C (2019) Sur la fanfaniite de Font Andreu, Argèles-sur-Mer (Pyrénées-Orientales). *Cahier des Micromonteurs* 24-27.
91. Cooper MA, Raade G, Ball NA, Abdu YA, Hawthorne FC, et al. (2018) Folvikite, $\text{Sb}^{5+}\text{Mn}^{3+}(\text{Mg,Mn}^{2+})_{10}\text{O}_8(\text{BO}_3)_4$, a new oxyborate mineral from the Kitteln mine, Nordmark ore district, Värmland, Sweden: description and crystal structure. *Mineral Mag* 82: 821-836.
92. Kampf AR, Plášil J, Nash BP, Marty J (2017) Greenlizardite, IMA 2017-001. *CNMNC Newsletter No. 37. Mineral Mag* 81: 737-742.

93. Plášil J, Kampf AR, Sejkora J, Čejka J, Škoda R, et al. (2018) Horákite, a new hydrated bismuth uranyl-arsenate-phosphate mineral from Jáchymov (Czech Republic) with a unique uranyl-anion topology. *J Geol* 63: 265-276.
94. Halenius U, Hatert F, Pasero M, Mills SJ (2018) New minerals and nomenclature modifications approved in 2018. *Mineral Mag* 82: 779-785.
95. Yakovenchuk VN, Ivanyuk GYu, Pakhomovsky YaA, Panikorovskii TL, Britvin SN, et al. (2018) Kampelite, $Ba_3Mg1.5Sc4(PO_4)6(OH)_3 \cdot 4H_2O$, a new very complex Ba-Sc phosphate mineral from the Kovdor phoscorite-carbonatite complex (Kola Peninsula, Russia). *Mineral Petrol* 102735240.
96. Mikhailenko DS, Korsakov AV, Rashchenko SV, Seryotkin YV, Belakovskiy DI, et al. (2018) Kuliginite, a new hydroxychloride mineral from the Udachnaya kimberlite pipe, Yakutia: Implications for low-temperature hydrothermal alteration of the kimberlites. *Amer Miner* 103: 1435-1444.
97. Subbotin VV, Vymazalová A, Laufek F, Savchenko YE, Stanley CJ, et al. (2019) Mitrofanovite, Pt_3Te_4 , a new mineral from the East Chuarvy deposit, Fedorovo–Pana intrusion, Kola Peninsula, Russia. *Mineral Mag* 83: 523-530.
98. Vignola P, Rotiroti N, Hatert F, Dal Bo F, Gentile P, et al. (2018) Plumbopharmacosiderite, $Pb_{0.5}Fe_3+4(AsO_4)_3(OH)_4 \cdot 5H_2O$, a new mineral species from the Monte Falò Pb-Zn mine near the village of Coiromonte in the Armeno municipality, Novara province, Italy. *Canad Mineral* 56: 143-150.
99. Campostrini I, Demartin F, Scavini M (2019) Russoite, $NH_4ClAs_2^{3+}O_3(H_2O)_{0.5}$, a new phylloarsenite mineral from Solfatara Di Pozzuoli, Napoli, Italy. *Mineralogical Magazine* 83: 89-94.
100. Chukanov NV, Rastsvetaeva RK, Kruszewski Ł, Aksenov SM, Rusakov VS, et al. (2018): Siudaite, $Na_8(Mn^{2+}_2Na)Ca_6Fe^{3+}_3Zr_3NbSi_{25}O_{74}(OH)_2Cl \cdot 5H_2O$: a new eudialyte-group mineral from the Khibiny alkaline massif, Kola Peninsula. *Phys Chem Miner* 45: 745-758.
101. Plášil J, Kampf AR, Meisser N, Lheur C, Brunsperger T, et al. (2020) Smamite, $Ca_2Sb(OH)_4[H(AsO_4)_2] \cdot 6H_2O$, a new mineral and a possible sink for Sb during weathering of fahlore. *Amer Miner* 105: 555-560.
102. Mauro D, Biagioni C, Bonaccorsi E, Halenius U, Pasero M, et al. (2019) $Fe_3+4(PO_4)_3(SO_4)(OH)(H_2O)_{10-n} \cdot nH_2O$, a new hydrated iron phosphate-sulfate. *Eur J Mineral* 31: 1033-1046.